Acc. Chem. Res. **2002,** *35,* 1018−1025

Fundamental Electronic Properties and Applications of Single-Walled Carbon Nanotubes

MIN OUYANG,† JIN-LIN HUANG,† AND CHARLES M. LIEBER*,†,‡

Department of Chemistry and Chemical Biology and Division of Engineering and Applied Science, Harvard University, Cambridge, Massachusetts 02138

Received February 13, 2002

ABSTRACT

Recent scanning tunneling microscopy studies of the intrinsic electronic properties of single-walled carbon nanotubes (SWNTs) are overviewed in this Account. A brief theoretical treatment of the electronic properties of SWNTs is developed, and then the effects of finite curvature and broken symmetry on electronic properties, the unique one-dimensional energy dispersion in nanotubes, the interaction between local spins and carriers in metallic nanotubes systems, and the atomic structure and electronic properties of intramolecular junctions are described. The implications of these studies for understanding fundamental one-dimensional physics and future nanotube device applications are also discussed.

I. Introduction

Single-walled carbon nanotubes (SWNTs) represent a new class of materials for investigating fundamental one-dimensional (1D) physics and for exploring nanoelectronics and molecular electronics.[1−4] Among the many interesting properties exhibited by nanotubes,[1] it is the electronic properties of SWNTs that are arguably the most significant characteristic of this new material. A single SWNT can be either metallic or semiconducting,[5−11] depending only on diameter and chirality, while the local carbon−carbon bonding remains constant. The ability to yield both metallic and semiconducting SWNTs without doping is unique among solid-state materials and has led to speculation that SWNTs might thus serve as a key building block for carbon-based electronics.[4]

Scanning tunneling microscopy (STM) is a powerful tool for probing the intrinsic electronic properties of SWNTs since both the atomic and electronic structures can be determined simultaneously for individual SWNTs.[9−11] Herein, we review recent STM investigations of the fundamental electronic properties of SWNTs and related nanoelectronic devices. First, a brief description of the basic relationship between the structure and electronic properties of SWNTs is presented. Second, the roles of finite curvature and broken symmetry in perturbing the electronic properties of SWNTs are discussed. Third, studies probing the unique one-dimensional energy dispersion of SWNTs are presented. Fourth, the interactions between local spins of external magnetic impurities and conduction electrons in both extended and finite metallic SWNTs are described. Last, characterization of several types of intramolecular SWNT junctions are presented. In concluding, the implications of these studies for understanding fundamental 1D physics and future device applications are considered.

II. Theoretical Background and Initial STM Studies

A SWNT can be viewed as a seamless cylinder obtained by rolling-up a section of a two-dimensional (2D) graphene sheet (Figure 1A). The structure of a SWNT is uniquely characterized by the roll-up vector, $\mathbf{C}_h = n\mathbf{a}_1 + m\mathbf{a}_2 \equiv (n,m)$, where $\mathbf{a}_1$ and $\mathbf{a}_2$ are the graphene primitive vectors and n,m are integers (Figure 1B). The translation vector, $\mathbf{T}$, is directed along the SWNT axis and perpendicular to $\mathbf{C}_h$; the magnitude of $\mathbf{T}$ corresponds to the length of the (n,m) SWNT unit cell. Once (n,m) is specified, other structural properties, such as diameter (d_t) and chiral angle (θ), can be determined: $d_t = (3^{1/2}/\pi)a_{cc}(m^2 + mn + n^2)^{1/2}$ and $\theta = \tan^{-1}[3^{1/2}m/(2n + m)]$, where a_{cc} is the nearest-neighbor carbon atom distance of 0.142 nm. Among the large number of possible $\mathbf{C}_h$ vectors, there are two inequivalent high-symmetry directions. These are termed "zigzag" and "armchair" and are designated by $(n,0)$ and (n,n), respectively.

The basic electronic band structure of SWNTs can be derived from a graphene sheet while neglecting hybridization effects due to the finite curvature of the tube structure. Graphene is a semimetal with valence and conduction bands degenerate at only six corners ($\mathbf{K}_B$) of the hexagonal first Brillouin zone. The Fermi surface of the graphene sheet is thus reduced to these six points (Figure 2A,B).[12] In SWNTs, the wavevector $\boldsymbol{k}$ is quantized along the circumferential direction due to periodic bound-

Min Ouyang was born in Fujian, China. He received B.S. and M.S. degrees in electronics from Peking University, and a Ph.D. in physical chemistry under the supervision of Charles Lieber from Harvard University in 2001. Ouyang's research interests focus on the fundamental properties and device applications of low-dimensional materials. He is currently pursuing postdoctoral research in physics with David Awschalom at the University of California, Santa Barbara.

Jin-Lin Huang received his undergraduate and doctoral degrees in physics from Fudan University. He joined Charles Lieber's group at Columbia University in 1989 as a postdoctoral fellow and is currently a research associate in the group at Harvard. Huang is interested in the basic physics of low-dimensional electronic systems and nanostructures, with specific emphasis on the development and application of low-temperature ultrahigh vacuum scanning tunneling microscopy to these systems.

Charles M. Lieber attended Franklin and Marshall College for his undergraduate education, and after doctoral studies at Stanford University and postdoctoral research at the California Institute of Technology, started his independent career in 1987 at Columbia University. Lieber moved to Harvard University in 1991, and now holds a joint appointment in the Department of Chemistry and Chemical Biology, where he is the Mark Hyman Professor of Chemistry, and the Division of Engineering and Applied Sciences. Lieber's research is focused broadly on nanoscale science and technology, including the rational synthesis, fundamental physical properties, and hierarchical organization of nanoscale materials, as well as the development of functional nanoelectronic and photonic systems.

* To whom correspondence should be addressed at the Department of Chemistry and Chemical Biology, Harvard University, 12 Oxford St., Cambridge, MA 02138. Phone: 617-496-3169. Fax: 617-496-5442/6731. E-mail: cml@cmliris.harvard.edu.

† Department of Chemistry and Chemical Biology.

‡ Division of Engineering and Applied Science.

10.1021/ar0101685 CCC: $22.00
Published on Web 08/15/2002

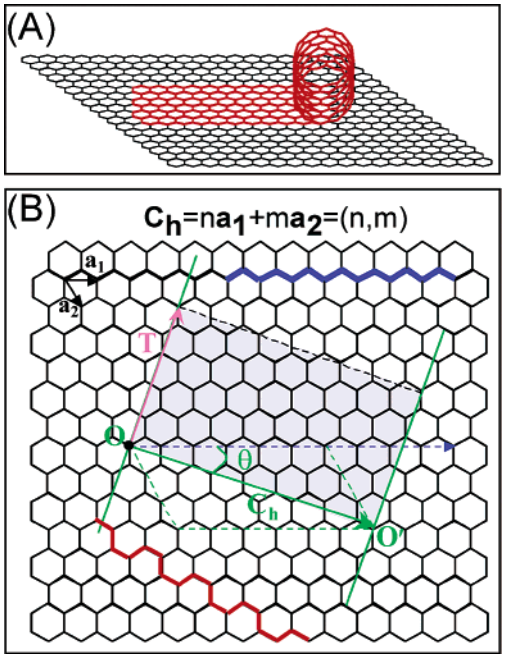

FIGURE 1. (A) Schematic of the roll-up of a graphene sheet to form a SWNT structure. (B) OO′ defines the chiral vector $\mathbf{C}_h = n\mathbf{a}_1 + m\mathbf{a}_2 \equiv (n,m)$. Translation vector, **T**, is along the nanotube axis and perpendicular to $\mathbf{C}_h$. The shaded, area represents the unrolled unit cell formed by **T** and $\mathbf{C}_h$. The chiral angle, θ, is defined as the angle between the $\mathbf{C}_h$ and the $(n,0)$ zigzag direction. $(n,0)$ zigzag and (n,n) armchair SWNTs are indicated in blue and red, respectively.

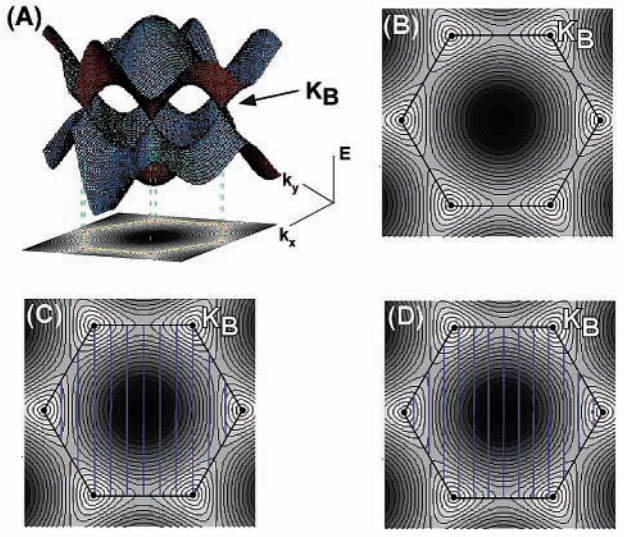

FIGURE 2. (A) Three-dimensional plot of the π and π^* graphene energy bands and (B) a 2D projection. (C) Allowed 1D wavevectors for a metallic (9,0) SWNT. (D) Allowed 1D wavevectors for a semiconducting (10,0) tube. The black hexagons define the first Brillouin zone of a graphene sheet, and the black dots in the corners are the $\mathbf{K}_B$ points. Blue lines represent allowed wavevectors, $\boldsymbol{k}$, within the first Brillouin zone.

ary condition: $\boldsymbol{k}\cdot\mathbf{C}_h = 2\pi q$, where q is an integer. Therefore, only a particular set of states, which are parallel to the corresponding tube axis with a spacing of $2/d_t$, are allowed (Figure 2C,D). On the basis of this simple scheme, if one of the allowed wavevectors passes through a Fermi $\mathbf{K}_B$ of the graphene sheet, the SWNT should be metallic, and otherwise it should be semiconducting. From the criteria $\mathbf{K}_B\cdot\mathbf{C}_h = 2\pi q$, we thus expect that SWNTs are metals when $(n - m)/3$ is an integer, and otherwise they are semiconductors.

The 1D band structure of SWNTs can be further constructed by zone-folding the 2D graphene band structure into the 1D Brillouin zone of an (n,m) SWNT, and the electronic density of states (DOS) can be computed from the band structure by summing the number of states at every energy level.[1,13] Several important characteristics of the electronic properties of SWNTs can be immediately obtained from this π-only tight binding model.[3,14−16] First, SWNTs exhibit well-defined spike-like features in the DOS, that is, van Hove singularities (VHS).[17] Second, the DOS at E_F is zero for semiconducting SWNTs ($n - m \neq 3q$) but nonzero (albeit small) for metallic SWNTs ($n - m = 3q$). Third, the VHS spacing has a characteristic "1−2−4" pattern relative to E_F (with spacing $1\xi-2\xi-4\xi$) for semiconducting SWNTs, and "1−2−3" from E_F (with spacing $3\xi-6\xi-9\xi$) for metallic SWNTs, where $\xi = 2\pi/3|\mathbf{C}_h|$. Fourth, the first VHS band gaps for semiconducting and metallic SWNTs are $E_g^S = 2\gamma_0 a_{cc}/d_t$ and $E_g^M = 6\gamma_0 a_{cc}/d_t$, respectively, and are independent of chiral angle θ to first order.

The first experiments that addressed directly these basic theoretical predictions were carried out by Odom et al.[9] and Wildöer et al.[10] using low-temperature STM. These initial STM studies characterized the atomic structures and electronic DOS of SWNTs, and thereby confirmed the existence of both semiconducting and metallic SWNTs for a wide range of structures. Subsequently, Kim et al.[13] and Odom et al.[3] reported the first detailed comparisons of experimentally determined SWNT VHS with tight binding calculations for metallic and semiconducting tubes. The good agreement between theory and these experiments showed that the essential physics of SWNT band structure is captured by the π-only model. However, other important issues, such as the effects of finite curvature and broken rotational symmetry, which are essential to a complete understanding of SWNTs' electronic properties and potential device applications, were not addressed. We examine these and other fascinating questions below.

III. Finite Curvature Effect of SWNTs

For a SWNT with sufficiently small diameter, the hybridization of σ, σ^*, π, and π^* orbitals can be quite large.[18] Full-valence tight binding calculations[19] and analytical calculations for a Hamiltonian on a curved surface[20] have suggested that the finite curvature of SWNTs will strongly modify the electronic behavior of SWNTs and open up small energy gaps at E_F. Recently, Ouyang et al.[11,21] and Kleiner et al.[22] have independently developed a Fermi-point shifting model to provide a direct understanding of finite curvature effects. Briefly, in this model, the finite curvature is found to induce shifts of the Fermi points of SWNTs from original $\mathbf{K}_B$ (Figure 3). For example, the Fermi points of "metallic" zigzag SWNTs are found to shift away

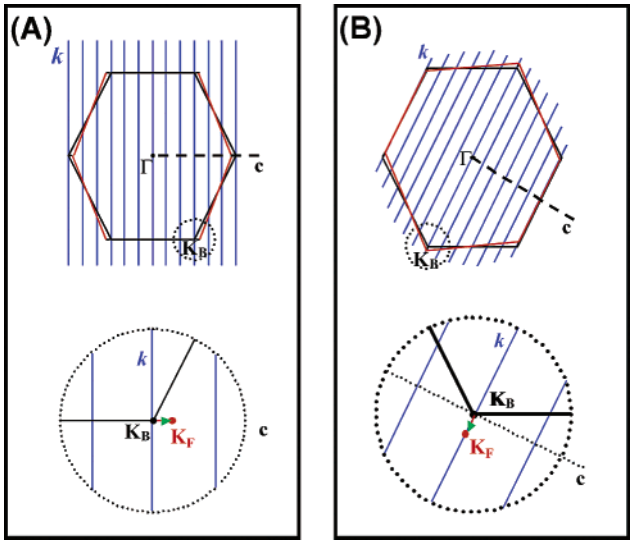

FIGURE 3. (A) (Top) The hexagonal Brillouin zone of the graphene sheet is defined by black lines. Blue lines are the allowed wavevectors, $\boldsymbol{k}$, of (9,0) zigzag SWNT, and red lines represent the effect of curvature. **c** is the circumferential direction perpendicular to the tube axis. (Bottom) Fermi point shift is indicated in red for a "metallic" zigzag SWNT; $\boldsymbol{k}_F$ moves along the **c** direction away from the $\mathbf{K}_B$ point. (B) Same as (A) but for an armchair SWNT. In this case, $\boldsymbol{k}_F$ moves along the tube axis.

from the $\mathbf{K}_B$ points along the circumference direction (Figure 3A), while the Fermi points of armchair SWNTs shift along the tube axis (Figure 3B). The shifts in zigzag tubes imply that wavevectors predicted to yield "metallic" zigzag SWNTs will no longer pass through the shifted Fermi points, and hence a small gap with $E_g^c = [3\gamma_0 a_{cc}^2/(16R^2)]$[19−22] will form in the DOS. In contrast, an isolated armchair SWNT will remain truly metallic because the shift occurs along the allowed wavevector.

Ouyang et al. carried out the first direct studies of curvature-induced gaps in SWNTs using low-temperature STM.[11] Figure 4A shows a typical atomically resolved image of a (15,0) SWNT. The VHS determined experimentally and calculated using a π-only tight binding model show excellent agreement (Figure 4B) and suggest that finite curvature does not perturb the larger energy features of the SWNT electronic structure. However, these data also showed a gaplike feature near E_F. High-resolution normalized tunneling spectra (inset in Figure 4B), which are proportional to the local DOS, clearly show that the local DOS at E_F are reduced to zero (i.e., a true energy gap), with gap width well fitted with the above predicted $1/R^2$ dependence.[11,21] The single fitting parameter used in this study, $\gamma_0 = 2.6$ eV, was also found to be in good agreement with the values determined in earlier STM studies.[9,10] In summary, these experimental studies have shown conclusively that previously predicted "metallic" $(n,0)$ SWNTs are actually narrow gap semiconductors.

IV. Broken Symmetry Effect of Armchair SWNTs

As discussed in the previous section, finite curvature will not affect the metallic nature of isolated armchair SWNTs due to their high symmetry. This suggestion is consistent

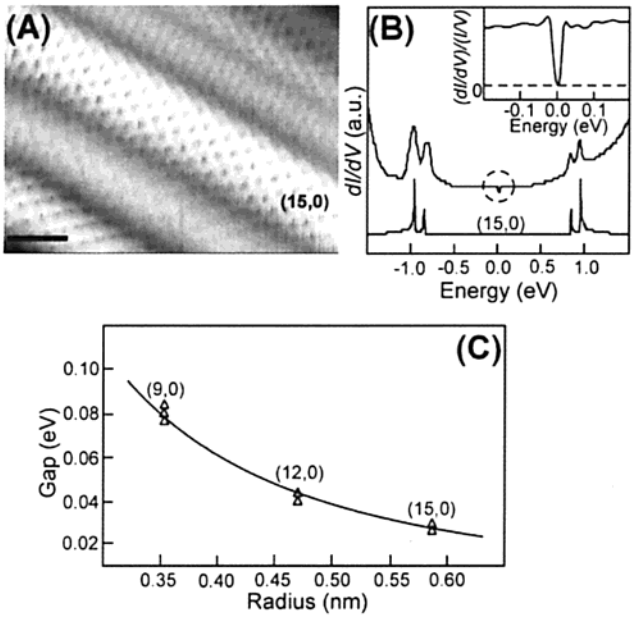

FIGURE 4. (A) Atomically resolved STM image of a (15,0) SWNT; scale bar, 1 nm. (B) Tunneling conductance, dI/dV, for (15,0) zigzag SWNTs, with corresponding calculated DOS shown below. The new feature near E_F is highlighted with a dashed circle. (Inset) High-energy resolution normalized conductance, $(dI/dV)/(I/V)$, for the (15,0) tube. (C) Curvature-induced energy gaps versus tube radius. Every data point (△) represents the averaged gap value for one distinct $(n,0)$ SWNT. The solid line corresponds to a fit with $E_g^c = 3\gamma_0 a_{cc}^2/(16R^2)$.

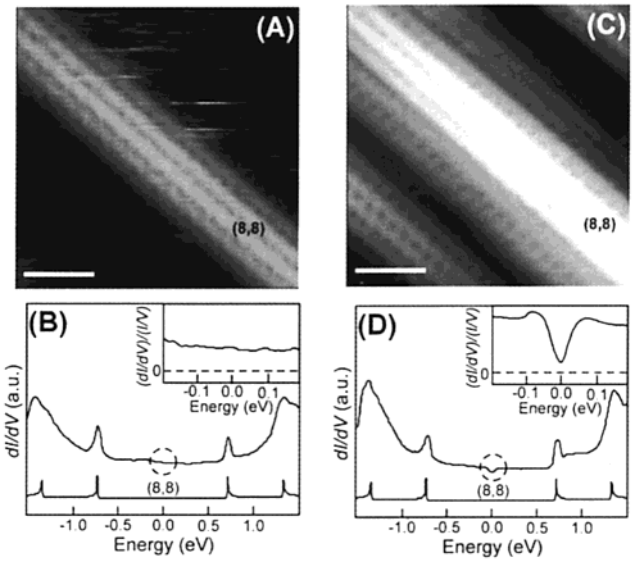

FIGURE 5. (A) STM image of an isolated (8,8) SWNTs on Au(111) substrate; scale bar, 1 nm. (B) (dI/dV) recorded on the isolated (8,8) tube. The calculated DOS for an isolated (8,8) tube is displayed below the experimental data. The dashed circle highlights the energy near E_F. (Inset) High-resolution $(dI/dV)/(I/V)$ data near E_F. (C) STM image of an (8,8) SWNT exposed at the top of a bundle; scale bar, 1 nm. (D) Same as (B) but data recorded on (8,8) tube in the bundle of (C). Adapted from refs 11 and 21.

with experimental data shown in Figure 5A. For this isolated (8,8) SWNT, the measured DOS was nonzero and constant at E_F, as expected for a metallic system (Figure 5B).[11] However, theories[14,23−25] also predict that if the

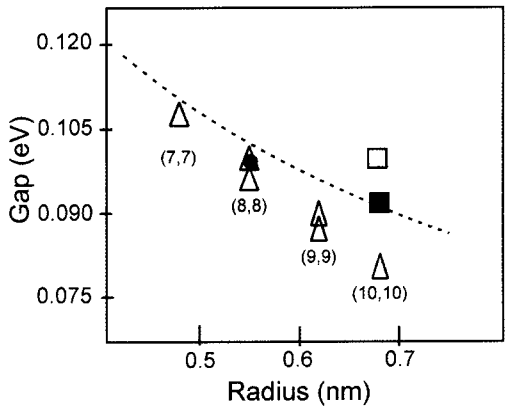

FIGURE 6. Summary of the observed pseudo gaps versus tube radius. Each experimental data point (△) represents an average gap value measured on a distinct (*n*,*n*) tube. Theoretical results are also shown for comparison: the solid square and dashed line correspond, respectively, to the gap value of a (10,10) tube and radius dependence of the gap widths from ref 24; the open square is for a (10,10) tube from ref 23. The solid circle shows the value calculated for an (8,8) tube from ref 14.

n-fold rotational symmetry of an armchair SWNT is broken, for example by tube−tube interactions within a tightly packed bundle, a gap will open at E_F and strongly reduce the conductance of the armchair SWNT. Odom et al.[3] and Ouyang et al.[11] first reported the existence of energy gap features near E_F in armchair SWNTs bundles. For example, the local DOS measured for an (8,8) SWNT packed in the bundle (Figure 5C,D) show a clear suppression around E_F, in contrast to the data for the isolated (8,8) SWNT. Experiments also suggested that these intertube interactions do not perturb the electronic band structure on a large energy scale (>0.1 eV) because both isolated and bundled tubes show similar VHS features.

The detailed gap structure observed in bundle armchair SWNTs (inset in Figure 5D) differs from the curvature-induced gaps in that the local DOS are largely suppressed but not reduced to zero; for this reason, these gaps are termed "pseudo gaps".[11] Similar gap features were observed in other armchair SWNT bundles,[21] with gap values ranging from 80 to 100 meV in the (10,10) through (7,7) SWNTs, respectively (Figure 6). These experimental pseudo gap widths fall within the same range as theoretical predictions. Particularly, our experimental data exhibit a weak inverse dependence on the SWNT radius, which is qualitatively consistent with theoretical predictions.[24] However, deviations between experiment and theory are also clear when making detailed comparisons. One possible origin for these differences is that STM experiments were carried out on SWNTs at the surfaces of bundles, while most theoretical calculations have been based on periodic lattices with higher local coordination. Future calculations carried out on structures accurately modeling STM experiments should help to address such differences.

Our experiments also have several important implications. First, the experimental observation of truly 1D metallic behavior in isolated armchair SWNTs on Au (111) substrate implies that the tube−Au substrate interaction does not strongly perturb the band structure.[3] Second, the presence of sizable pseudo gaps in armchair tube bundles will modify electrical transport, and the very low DOS at E_F will make extended states in such tubes susceptible to localization. From a positive perspective, the existence of pseudo gaps in armchair SWNTs should make these samples sensitive to doping and could enable their applications as nanosensors.

V. Energy Dispersion of Armchair SWNTs

SWNTs are predicted to exhibit a unique linear energy dispersion at low energies ($E/\gamma_0 \ll 1$), which contrasts the parabolic dependence expected from a conventional free-electron picture and will define the behavior of electrons near E_F.[15] However, experimental determination of this unique feature of the band structure has been lacking.

Ouyang et al. first applied the STM to elucidate the 1D energy dispersion of SWNTs by characterizing in detail energy-dependent quantum interference of electrons scattered by defects in metallic nanotubes.[26] Defects in metallic tubes are frequently found to induce modulations in the DOS with a period larger than that of the normal nanotube lattice.[26,27] In the specific example shown in Figure 7, tunneling spectra as well as atomically resolved images recorded away from the defect (∼8 nm) clearly identify that this tube is an isolated (13,13) SWNT.[21,26] In contrast, tunneling spectra recorded near the defect region show nine new low-energy peaks within the first VHS peaks[21,26] and demonstrate that the amplitude of these peaks oscillates along the tube axis (Figure 7).

The oscillations in the DOS at specific energies can be understood in terms of resonant electron scattering from defect-related quasi-bound states, which has been reported in recent SWNT theoretical studies[28] and transport measurements.[29] From this picture, Ouyang et al. modeled the energy-dependent oscillations as the interference between an incident 1D plane wave, e^{ikx} (where x is position), of energy equal to that of a defect quasi-bound state and the resonantly backscattered electrons with reflectivity $|R|^2$ ($R = |R|e^{-i\delta}$, where δ is the phase shift). This approach leads to an expression for the spatial oscillation in the DOS: $\rho(k,x) = 1 + |R|^2 + 2|R| \cos(2kx + \delta)e^{-2x/l\varphi}$, where l_φ is the phenomenological phase coherence length used to account for inelastic scattering processes.[26]

This model provides excellent fits to the energy-dependent oscillatory data (Figure 7)[26] and further yields the energy dispersion, $E(k)$ vs k (Figure 8A). Significantly, these data show that the dispersion is, indeed, linear near E_F and agree well with the relationship predicted for armchair SWNTs, $|E(k)| = (3/2)a_{cc}\gamma_0|k - k_F|$.[15] These fits also yield a value of $\gamma_0 = 2.51$ eV that is in good agreement with previous experimental values from STM studies,[9−11] and a value of $k_F = 8.48 \pm 0.05$ nm^{-1} that is also consistent with the predicted value, $k_F = 2\pi/(3^{3/2}a_{cc}) = 8.52$ nm^{-1}, for an armchair SWNT.[1]

Lemay et al. also recently reported an STM study of 1D energy dispersions in metallic SWNTs by imaging the wave functions in finite size (∼40 nm) nanotubes.[30] The

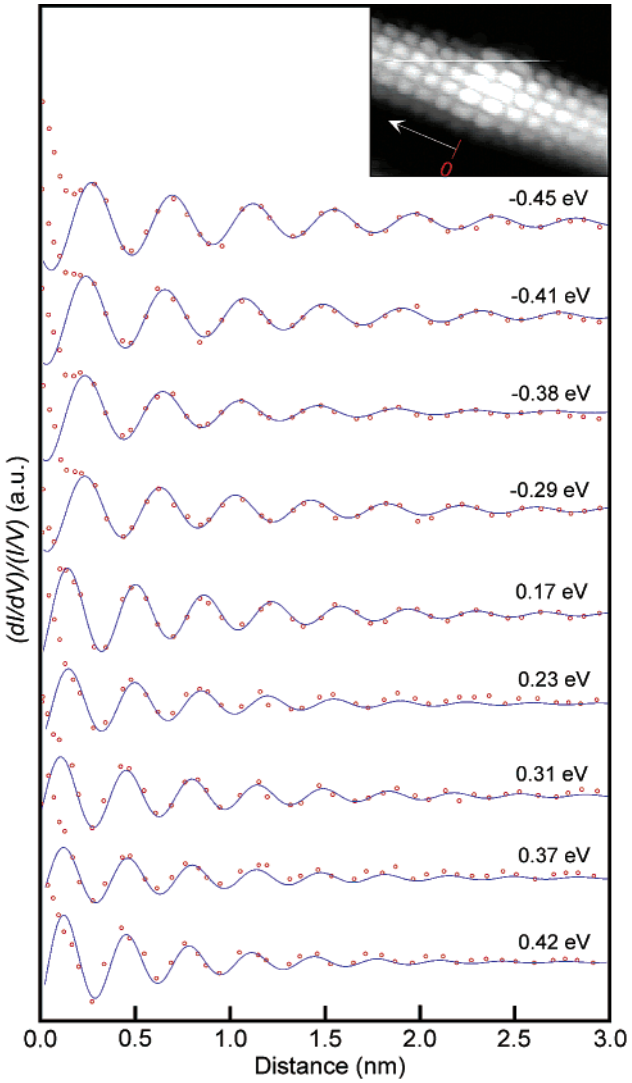

FIGURE 7. Spatial oscillation of $(dI/dV)/(I/V)$ at different energies. (Inset) Atomically resolved image of an isolated (13,13) armchair SWNT containing one defect whose position is highlighted with a red line. The origin represents the defect position, which corresponds to the red mark in the inset, and the distance is along the tube axis (white arrow, inset). Red open circles: experimental data. Blue solid lines: fit with $\rho(k,x) = 1 + |R|^2 + 2|R| \cos(2kx + \delta)e^{-2x/l_\varphi}$.

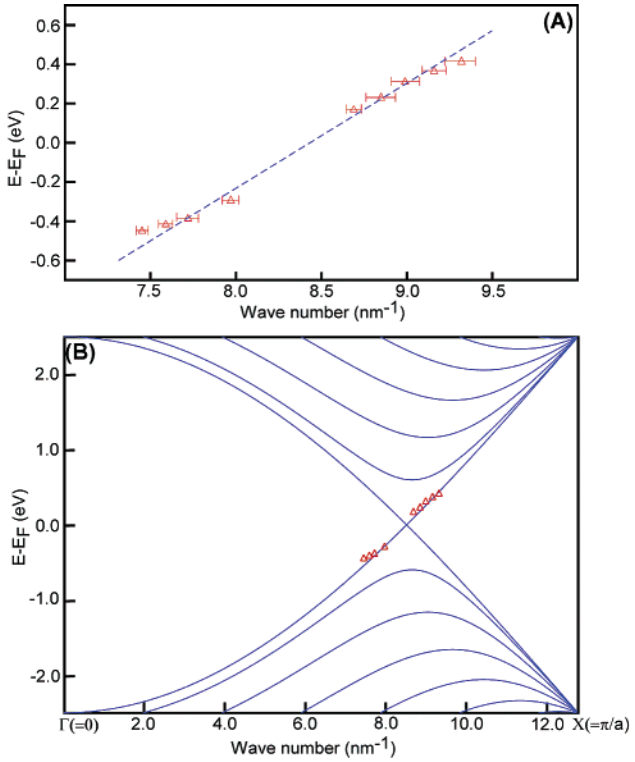

FIGURE 8. (A) Energy dispersion near E_F for the (13,13) armchair SWNT. The experimental data points (red triangles) fall on a line defined by $|E(k)| = (3^{1/2}/2)a\gamma_0|k - k_F|$. (B) Band structure for a (13,13) armchair SWNT plotted along the Γ−X line (blue solid lines) and experimental $E(k)$ vs k data points (red triangles). Adapted from ref 26.

physical principle behind this study is the same as that in our quantum interference method: the ~40 nm long tubes can be taken as the system with two defects (both ends) that reflect two pairs of Bloch waves. However, this study focused on chiral tubes packed in a bundle and neglected the significant effects of finite curvature and tube−tube interactions reviewed above.

One interesting but important issue further raised by Ouyang et al. is the relationship between the defect parity and the symmetry of the energy bands in armchair SWNTs. Comparison of the experimental energy dispersion with the band structure calculated for a (13,13) SWNT (Figure 8B) demonstrates that our experimental data are in excellent agreement with the calculated π^* band, although no data overlap with the π band.[26] The absence of the π band can be understood in terms of parity matching.[31] Briefly, the π and π^* bands of armchair SWNTs have opposite parity,[15] and thus if the defect in Figure 7A has odd parity, then electrons in the π band (even parity) will not be scattered by the defect, whereas electrons in the π^* band (odd parity) can be scattered when their energies match a defect quasi-bound state. Although more experiments are needed to provide a deeper understanding of this important issue, we believe that this new work highlights the potential of resonant scattering as an approach for investigating fundamental issues of parity and symmetry breaking in 1D SWNTs and nanowires.

VI. Kondo Phenomena in 1D SWNTs

SWNTs provide exciting opportunities to study other fundamental issues in 1D electron hosts. For example, the availability of SWNTs enables one to probe how 1D electron systems interact with magnetic impurities, that is, the Kondo effect in 1D. The Kondo effect, which describes the interaction between a local magnetic moment of a magnetic impurity and conduction electrons of a nonmagnetic host, is a well-known phenomenon that leads to anomalous transport behavior in bulk systems of dilute magnetic alloys.[32] Briefly, at low temperature the electrons of the host tend to screen the local spin of the magnetic impurity, resulting in a change of the local DOS at E_F around the site of the magnetic impurity, i.e., the emergence of a Kondo resonance.[33] The Kondo resonance should disappear above the Kondo temperature, T_K, which characterizes the interaction strength. In STM experi-

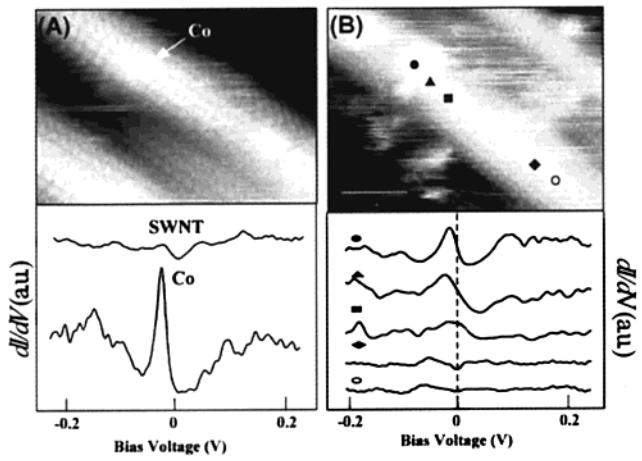

FIGURE 9. (A) Atomically resolved image of a 0.5 nm Co cluster on a SWNT, and *dI*/d*V* versus *V* recorded at the position of the Co cluster and ~7 nm away from the cluster. (B) Constant current image of a larger Co cluster (~1 nm) on a SWNT, and corresponding *dI*/d*V* versus *V* measured at points indicated in the image. Adapted from refs 21 and 38.

ments, electrons can tunnel from the tip into both the localized orbital of the magnetic impurity and the continuum states of the conduction electrons. The final state of the electron can occupy two energetically degenerate states, and thus leads to quantum interference that can be described with a Fano model.[34] This Fano resonance at E_F will appear as either a symmetric antiresonance or an asymmetric resonance, depending upon the details of the interference. The Kondo resonance for 2D systems was recently observed in STM investigations of magnetic atoms on noble metal surfaces.[35−37]

Odom et al. first studied the interaction between the local spin of Co clusters and extended and finite size SWNTs.[38] STM images showed that Co clusters could be readily observed on atomically resolved metallic SWNT (Figure 9), and spectroscopy data recorded directly above the cluster exhibited a strong resonance peak near E_F. Spatially resolved measurements further showed that these peak features systematically decrease in amplitude and ultimately disappear after several nanometers. The new resonance peaks were not observed with nonmagnetic Ag clusters or with Co clusters on semiconducting SWNTs,[38] which suggested that the observed peak was due to the interaction of a magnetic spin with the SWNT conduction electrons. In addition, analyses of the resonance revealed new characteristics about the effect of dimensionality compared with 2D systems.[35−37] In 2D systems, the Kondo resonance is usually evident as a dip or antiresonance in the tunneling conductance, while in the measurement of Co on SWNTs, the Kondo resonance always appears as a sharp peak. This difference can be qualitatively understood in terms of the small number of "continuum" final states available for tunneling into a SWNT versus a noble metal surface in this two-channel quantum interference problem.[35−38]

Odom et al. also studied the Kondo effect in a very short metallic SWNT, where the energy level spacing of the conduction electrons was larger than k_BT_K (vs normally $\ll k_BT_K$ in extended systems),[39] by characterizing the DOS on and near Co clusters before and after cutting a SWNT host to ~11 nm. The spectra recorded after cutting not only resolved the expected discrete eigenstates separated by ~0.15 eV,[3,38] due to the quantum finite size effect, but also showed that the peak amplitude at E_F was markedly enhanced relative to those of the other level peaks. The enhanced conductance at E_F provides evidence of how sensitive the electronic properties of metallic nanotubes are to magnetic impurities, even in finite size structures where the level spacing is much larger than k_BT_K.

These initial studies suggest that metallic SWNTs are ideal hosts for studying the basic physics of the Kondo effect in 1D systems, although the magnetic clusters (<1 nm) explored in this first report[38] also complicate analysis compared to the ideal of a single atom spin center. In this regard, future studies of the 1D Kondo effect could benefit substantially by using single magnetic atoms or molecules that have well-defined (and controllable) spin and can be registered precisely with respect to the underlying SWNT atomic lattice.

VII. Intramolecular Junctions of SWNTs

SWNTs are also expected to play an important role in nanoscale device applications. An exciting idea in this regard is to create SWNT intramolecular junctions (IMJs). Theoretical work suggested early on that two different tubes could be connected seamlessly by interposing one or more pentagon−heptagon (5/7) topologic defects between two nanotube segments of different helicity.[40−43] Although transport measurements[44] provided indirect evidence for the existence of proposed IMJs, direct characterization of these potentially important structures was lacking until the recent work of Ouyang et al.[45]

Analysis of atomically resolved images has enabled the identification of IMJs.[45] For example, the data in Figure 10A show that the upper and lower portions of the nanotube have similar diameters (1.57 ± 0.07 nm) but significantly different chiral angles, where θ is −3.9° ± 0.8° and −10.5° ± 0.8° for upper and lower portions, respectively. Therefore, the SWNT indices of the upper and lower regions can be assigned as (21,−2) and (22,−5), respectively, and moreover, the interface between SWNTs can be further modeled (Figure 10B).[45] The spectroscopic evidence for the overall IMJ structure (Figure 10C) shows that the upper and lower portions correspond to a semiconductor and metal, respectively. Hence, these results demonstrate that the IMJ is a M−S junction—a basic building block for nanoelectronics.

Spatially resolved tunneling spectroscopy also enabled us to investigate the detailed interface properties of this and other IMJs. From the data shown in Figure 10C, this junction has a very sharp metal−semiconductor interface: the semiconducting VHS gap decays across the IMJ into the metallic segment within <1 nm, whereas the distinct spectroscopic features of the metallic tube appear

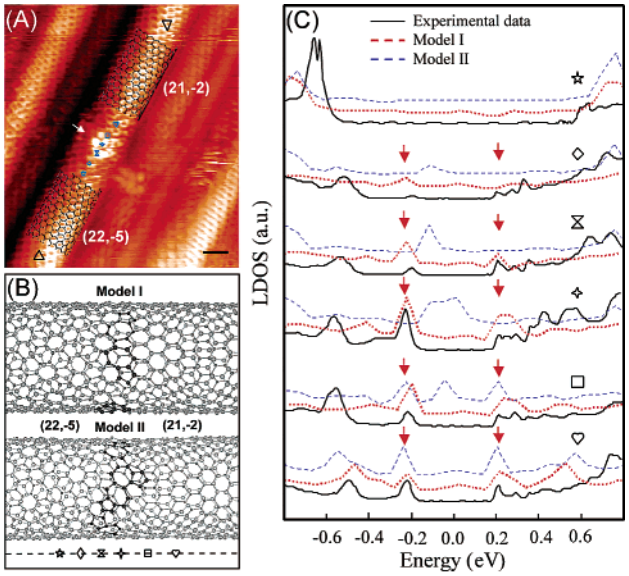

FIGURE 10. (A) Atomically resolved STM image of a SWNT containing an IMJ (white arrow). Black honeycomb meshes correspond to (21,−2) and (22, −5) models overlaid on the upper and lower portions, respectively, to highlight the distinct atomic structures of the different regions of the SWNT. Scale bar, 1 nm. (B) Model I has three separated 5/7 pairs, and model II has two isolated 5/7 pairs and one 5/7−7/5 pair. The solid black spheres highlight the atoms forming the 5/7 defects. (C) Solid line: spatially resolved *dI*/d*V* data acquired across the M−S IMJ at the positions indicated by six symbols in (A). Red dashed line: calculated local DOS for model **I**. Blue dashed line: calculated local DOS for model II. Arrows highlight features found in both model I and the data.

to decay more quickly across the junction interface. Ouyang et al. used atomic models of the interface to compare calculated and experimentally measured DOS of this IMJ. Two low-energy structural models (Figure 10B), containing three and four 5/7 pairs, respectively, were analyzed. Significantly, the local DOS (Figure 10C) obtained from tight binding calculations for model I agreed well with the measured local DOS across the IMJ interface, while model II exhibited low-energy states around −0.10 eV not observed in experiment. Hence, it was possible to assign the structure of model I as a reasonable representation for the observed (21,−2)−(22,−5) IMJ.

Similar direct and detailed characterization of metallic−metallic (M−M) IMJs has also been carried out,[45] and recently, much more complicated junction structures have been observed and studied.[46] For example, Figure 11A shows one single hybrid tube consisting of three different segments: armchair (11,11)−zigzag (19,0)−armchair (11,11). Spatially resolved spectroscopic measurements (Figure 11B) further support this structure, which is analogous to macroscopic metal−insulator−metal devices.[47] The ability to characterize directly the atomic structure and electronic properties of IMJs by STM has important implications for applications, since it provides a clear means for assessing synthetic efforts designed to prepare specific IMJs. We believe that such work could open up significant opportunity both for fundamental investigations of resonant scattering and for the controlled growth of intramolecular SWNT nanoelectronic devices.

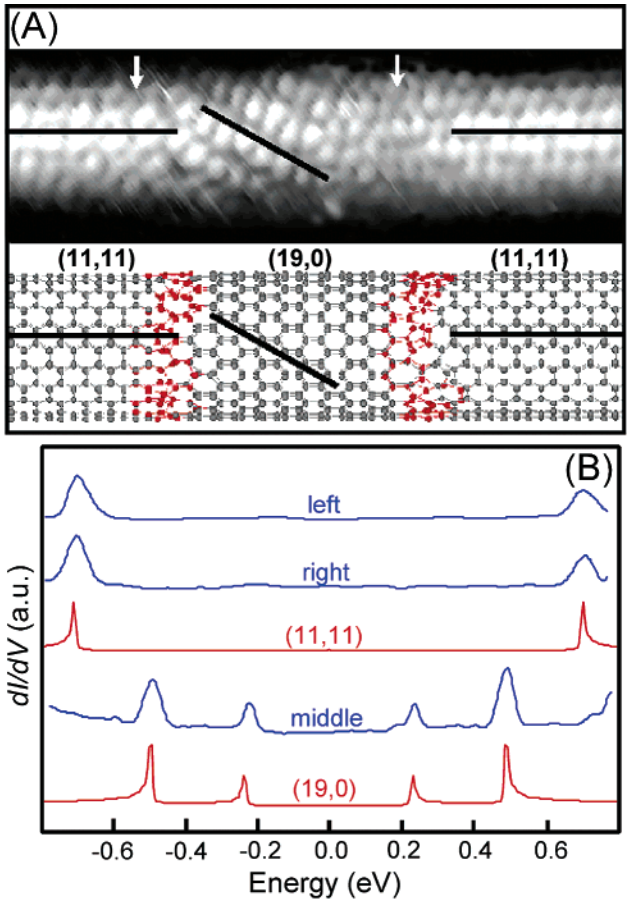

FIGURE 11. (A) (Top) Atomically resolved image of (11,11)−(19,0)−(11,11) structure. (Bottom) Model of (11,11)−(19,0)−(11,11) structure constructed with 5/7 pairs in the interfaces (highlighted in red). The black bold lines highlight different chiral directions in three different segments along the tube axis. (B) Blue curves: experimental data measured in the three different segments in (A). Red curves: calculated DOS for (11,11) and (19,0) SWNTs.

VIII. Concluding Remarks

Scanning tunneling microscopy has contributed significantly to our understanding of the fundamental structural and electronic properties of individual and bundled SWNTs. Studies of defect-free SWNTs have shown that the electronic properties of nanotubes depend not only on radius and chirality but also on their detailed curvature and local environment. Previously predicted "metallic" zigzag tubes are actually narrow gap semiconductors with gap magnitudes depending inversely on the square of the SWNT radius, whereas isolated armchair SWNTs do not have energy gaps and are truly metallic. In addition, armchair SWNTs in bundles exhibit large pseudo gaps at E_F due to tube−tube interactions. STM was also used to determine directly the unique linear 1D energy dispersion of SWNTs through the analysis of resonant scattering and quantum interference. As 1D systems, SWNTs were also used to study fundamental interactions between magnetic clusters and 1D electron hosts. Last, direct atomically resolved characterization of intramolecular junctions in as-grown SWNT samples by STM demonstrated the existence of IMJs and could have important implications for

the controlled introduction of defects for nanoelectronic device applications. In short, we believe that the results discussed in this paper open a window into this fascinating 1D system. Future efforts promise to be rewarded with answers to very fundamental scientific questions, and importantly, these results should push from a firm intellectual footing the application of SWNTs in future nanotechnologies.

We are indebted to our colleagues and collaborators. In particular, we thank Prof. H. Park, L. J. Lauhon, J. F. Wang, M. S. Gudiksen, and K. Kim for stimulating discussions, and we thank T. W. Odom, P. Kim and C. L. Cheung for their contributions to the work summarized herein. C.M.L. gratefully acknowledges support of this work by Solid State Chemistry and Chemistry Divisions of the NSF.

References

(1) See: Saito, R.; Dresselhaus, G.; Dresselhaus, M. *Physical properties of carbon nanotubes*; Imperial College: London, 1998.
(2) Dekker, C. Carbon Nanotubes as Molecular Quantum Wires. *Phys. Today* **1999**, *52*(5), 22−28.
(3) Odom, T. W.; Huang, J.-L.; Kim, P.; Lieber, C. M. Structures and Electronic Properties of Carbon Nanotubes. *J. Phys. Chem. B* **2000**, *104*, 2794−2809.
(4) McEuen, P. L. Carbon Based Electronics. *Nature* **1998**, *393*, 15−16.
(5) Mintmire, J. W.; Dunlap, B. J.; White, C. T. Are Fullerene Tubules Metallic? *Phys. Rev. Lett.* **1992**, *68*, 631−634.
(6) Hamada, N.; Sawada, S.; Oshiyama, A. New One-Dimensional Conductors: Graphitic Microtubules. *Phys. Rev. Lett.* **1992**, *68*, 1579−1582.
(7) Saito, R.; Fujita, M.; Dresselhaus, G.; Dresselhaus, M. Electronic Structure of Chiral Graphene Tubules. *Appl. Phys. Lett.* **1992**, *60*, 2204−2206.
(8) Saito, R.; Fujita, M.; Dresselhaus, G.; Dresselhaus, M. Electronic Structure of Graphene Tubules Based on C_{60}. *Phys. Rev. B* **1992**, *46*, 1804−1811.
(9) Odom, T. W.; Huang, J. L.; Kim, P.; Lieber, C. M. Atomic Structure and Electronic Properties of Single-Walled Carbon Nanotubes. *Nature* **1998**, *391*, 62−64.
(10) Wildöer, J. W. G.; Venema, L. C.; Rinzler, A. G.; Smalley, R. E.; Dekker: C. Electronic Structure of Atomically Resolved Carbon Nanotubes. *Nature* **1998**, *391*, 59−62.
(11) Ouyang, M.; Huang, J. L.; Cheung, C. L.; Lieber, C. M. Energy Gaps in "Metallic" Single-Walled Carbon Nanotubes. *Science* **2001**, *292*, 702−705.
(12) Wallace, P. R. The Band Theory of Graphite. *Phys. Rev.* **1947**, *71*, 622−634.
(13) Kim, P.; Odom, T. W.; Huang, J. L.; Lieber, C. M. Electronic Density of Atomically Resolved Single-Walled Carbon Nanotubes: van Hove Singularities and End States. *Phys. Rev. Lett.* **1999**, *82*, 1225−1228.
(14) Rubio, A. Spectroscopic Properties and STM Images of Carbon Nanotubes. *Appl. Phys. A* **1999**, *68*, 275−282.
(15) Mintmire, J. W.; Robertson, D. H.; White, C. T. Properties of Fullerene Nanotubules. *J. Phys. Chem. Solids* **1993**, *54*, 1835−1840.
(16) Mintmire, J. W.; White, C. T. Universal Density of States for Carbon Nanotubes. *Phys. Rev. Lett.* **1998**, *81*, 2506−2509.
(17) See: Ashcroft, N. W.; Mermin, N. D. *Solid State Physics*; Holt, Rinerhart and Winston: New York, 1976.
(18) Blasé, X. B.; Benedict, X.; Shirley, E. L.; Louie, S. G. Hybridization Effects and Metallicity in Small Radius Carbon Nanotubes. *Phys. Rev. Lett.* **1994**, *72*, 1878−1881.
(19) White, C. T.; Robertson, D. H.; Mintmire, J. W. In *Clusters and Nanostructures Materials*; Jena, P., Behera, S., Eds.; Nova: New York, 1996; pp 231−237.
(20) Kane, C. L.; Mele, E. J. Size, Shape, and Low Electronic Structure of Carbon Nanotubes. *Phys. Rev. Lett.* **1997**, *78*, 1932−1935.
(21) Ouyang, M.; Huang, J. L.; Lieber, C. M. Scanning Tunneling Microscopy Studies of the One-Dimensional Electronic Properties of Single-Walled Carbon Nanotubes. *Annu. Rev. Phys. Chem.* **2002**, *53*, 201−220.
(22) Kleiner, A.; Eggert, S. Band Gaps of Primary Metallic Carbon Nanotubes. *Phys. Rev. B* **2001**, *63*, 734081−734084.
(23) (a) Delaney, P.; Choi, H. J.; Ihm, J.; Louie, S. G.; Cohen, M. L. Broken Symmetry and Pseudogaps in Ropes of Carbon Nanotubes. *Nature* **1998**, *391*, 466−469. (b) Delaney, P.; Choi, H. J.; Ihm, J.; Louie, S. G.; Cohen, M. L. Broken Symmetry and Pseudogaps in Ropes of Carbon Nanotubes. *Phys. Rev. B* **1999**, *60*, 7899−7904.
(24) Maarouf, A. A.; Kane, C. L.; Mele, E. J. Electronic Structure of Carbon Nanotube Ropes. *Phys. Rev. B* **2000**, *61*, 11156−11165.
(25) Kwon, Y. K.; Saito, S.; Tomanek, D. Effect of Intertube Coupling on the Electronic Structure of Carbon Nanotube Ropes. *Phys. Rev. B* **1998**, *58*, 13314−13317.
(26) Ouyang, M.; Huang, J. L.; Lieber, C. M. Determination of One-Dimensional Energy Dispersion of Single-Walled Carbon Nanotubes by Resonant Electron Scattering. *Phys. Rev. Lett.* **2002**, *88*, 066804-1−066804-4 (cond-mat/0107580).
(27) Clauss, W.; Begeron, D. J.; Freitag, M.; Kane, C. L.; Mele, E. J.; Johnson, A. T. Electron Backscattering on Single-Wall Carbon Nanotubes Observed by Scanning Tunneling Microscopy. *Europhys. Lett.* **1999**, *47*, 601−607.
(28) Choi, H. J.; Ihm, J.; Louie, S. G.; Cohen, M. L. Defects, Quasibound States and Quantum Conductance in Metallic Carbon Nanotubes. *Phys. Rev. Lett.* **2000**, *84*, 2917−2920.
(29) Bockrath, M.; Liang, W.; Bozovic, D.; Hafner, J. H.; Lieber, C. M.; Tinkham, M.; Park, H. Resonant Electron Scattering by Defects in Single-Walled Carbon Nanotubes. *Science* **2001**, *291*, 283−285.
(30) Lemay, S. G.; Janssen, J. W.; van den Hout, M.; Mooij, M.; Bronlkowski, M. J.; Willis, P. A.; Smalley, R. E.; Kouwenhoven, L. P.; Dekker: C. Two-Dimensional Imaging of Electronic Wavefunctions in Carbon Nanotubes. *Nature* **2001**, *412*, 617−620.
(31) Mizes, H. A.; Foster, J. S. Long-Range Electronic Perturbations Caused by Defects Using Scanning Tunneling Microscopy. *Science* **1989**, *244*, 559−562.
(32) Kondo J, Resistance Minimum in Dilute Magnetic Alloys. *Prog. Theor. Phys.* **1964**, *32*, 37−87.
(33) See: Hewson, A. C. *The Kondo Problem to Heavy Ferminons*; Cambridge University Press: Cambridge, 1993.
(34) Fano, U. Pairs of Two-level Systems. *Rev. Mod. Phys.* **1983**, *55*, 855−874.
(35) Li, J.; Schneider, W. D.; Berndt, R.; Delley, B. Kondo Scattering Observed at a Single Magnetic Impurity. *Phys. Rev. Lett.* **1998**, *80*, 2893−1896.
(36) Madhavan, V.; Chen, W.; Jamneala, T.; Crommie, M. F.; Wingreen, N. S. Tunneling into a Single Magnetic Atom: Spectroscopic Evidence of the Kondo Resonance. *Science* **1998**, *280*, 567−570.
(37) Manoharan, H. C.; Lutz, C. P.; Eigler, D. W. Quantum Mirages Formed by Coherent Projection of Electric Structure. *Nature* **2000**, *403*, 512−515.
(38) Odom, T. W.; Huang, J. L., Cheung, C. L.; Lieber, C. M. Magnetic Clusters on Single-Walled Carbon Nanotubes: the Kondo Effect in a One-Dimensional Host. *Science* **2000**, *290*, 1549−1552.
(39) Thimm, W. B.; Kroha, J.; von Delft, J. Kondo Box: A Magnetic Impurity in an Ultrasmall Metallic Grain. *Phys. Rev. Lett.* **1999**, *82*, 2143-2146.
(40) Dunlap, B. I. Relating Carbon Tubules. *Phys. Rev. B* **1994**, *49*, 5643−5651.
(41) Saito, R.; Dresselhaus, G.; Dresselhaus, M. S. Tunneling Conductance of Connected Carbon Nanotubes. *Phys. Rev. B* **1996**, *53*, 2044−2050.
(42) Lambin, Ph.; Fonseca, A.; Vigneron, J. P.; Nagy, J. B.; Lucas, A. A. Structural and Electronic Properties of Bent Carbon Nanotubes. *Chem. Phys. Lett.* **1995**, *245*, 85−89.
(43) Chico, L.; Crespi, V. H.; Benedict, L. X.; Louie, S. G.; Cohen, M. L. Pure Carbon Nanoscale Devices: Nanotube Heterojunctions. *Phys. Rev. Lett.* **1996**, *76*, 971−974.
(44) Yao, Z.; Postma, H. W. Ch.; Balents, L.; Dekker, C. Carbon Nanotube Intramolecular Junctions. *Nature* **1999**, *402*, 273−276.
(45) Ouyang, M.; Huang, J. L.; Cheung, C. L.; Lieber, C. M. Atomically Resolved Single-Walled Carbon Nanotube Intramolecular Junctions. *Science* **2001**, *291*, 97−100.
(46) Ouyang, M.; Huang, J. L.; Lieber, C. M. Unpublished data.
(47) Orlikowski, D.; Nardelli, M. B.; Bernholc, J.; Roland, C. Ad-dimers on Strained Carbon Nanotubes: A New Route for Quantum Dot Formation? *Phys. Rev. Lett.* **1999**, *83*, 4132−4135.

AR0101685